Calculation of relative permeabilities of water and steam from laboratory measurements

Maria Gudjonsdottir [a,b,*], Halldor Palsson [b], Jonas Eliasson [b], Gudrun Saevarsdottir [a]

[a] School of Science and Engineering, Reykjavik University, Menntavegur 1, IS-101 Reykjavik, Iceland
[b] School of Engineering and Natural Sciences, University of Iceland, Saemundargata 2, IS-101 Reykjavik, Iceland

ARTICLE INFO

ABSTRACT

Measurements of two phase flow of water and steam in porous media were performed and relative permeabilities calculated. The goal was to compare the relative permeabilities from measurements using fluid of geothermal origin to known relative permeability curves, and to examine the effect of parameter variations. Due to high sensitivity to intrinsic (absolute) permeability, the data spread was large. Nevertheless, the Corey curves seem to be an appropriate curve for relative permeability functions. The results give insight into the behavior and characteristics of flashing of hydrothermal fluid in liquid dominated geothermal reservoirs.

© 2014 Elsevier Ltd. All rights reserved.

1. Introduction

The flow of a geothermal fluid through a geothermal reservoir resembles flow through porous material using Darcy's law as one of the governing equations. In reality, geothermal reservoirs normally consist of fractured rock with the inhomogeneous permeability of a fractured matrix (Grant and Bixley, 2011). On a macroscopic scale, the porous media assumption seems appropriate (Chen et al., 2004; Chen and Horne, 2006) and it is conventionally used to describe flow in geothermal reservoirs (Chen, 2005) although some reservoir modeling tools like TOUGH2 allow double porosity and dual permeability definitions for the reservoir structure (Pruess et al., 1999).

In general, for the common type of liquid dominated reservoirs (Axelsson, 2008), the geothermal fluid exists either as a single phase water or a mixture of water and steam. The geothermal fluid contains dissolved gasses and solids (Arnorsson et al., 2007), but is generally assumed to be pure water or steam when its flow through the permeable matrix is simulated (O'Sullivan et al., 2001). The two phase flow of water and steam occurs under different conditions. If the reservoir is liquid dominated, boiling can occur and a two phase mixture is formed (Axelsson, 2008). Such a system as suggested by White (1967) is described as a conceptual model, shown in Fig. 1. In the figure the heat source is assumed to be a magma intrusion at

few kilometers depth, conducting heat through impermeable layer to the porous and fractured matrix above.

Another mechanism resulting in two phase flow is where production wells are used to extract fluid from the reservoir for utilization. When the fluid is extracted through the wells, flashing occurs due to pressure drop in the well. The high enthalpy fluid reaches saturation through the pressure reduction and steam begins to form. The flashing horizon (the point where flashing starts) may either begin in the well or in the porous surroundings where the fluid is approaching the well (DiPippo, 2008). A schematic figure showing the geothermal reservoir and the well is shown in Fig. 2.

When two phase flow occurs through a porous matrix at a very low velocity, it results in a low Reynolds number making Darcy's law applicable (Todd and Mays, 2005). Note that Darcy's original law represents a single phase flow but an adaptation to a multi-phase flow is possible by using the concept of relative permeability.

Several relations for relative permeabilities are found in the literature (Pruess et al., 1999), normally showing them as functions of the water saturation, that is the portion of the total pore space in the flow channel occupied by water. These relations have been found experimentally and many of them originate from the oil and gas industry where the two phases are different immiscible substances rather than a single substance, but have also been adopted to geothermal reservoirs.

Results from previous experiments involving water and steam for determining relative permeabilities are found in literature. A number of them are summarized in Table 1 where the parameters for the experimental procedure are listed and the resulting relative

* Corresponding author at: Reykjavik University, Menntavegur 1, IS-101 Reykjavik, Iceland. Tel.: + 354 599 6200.
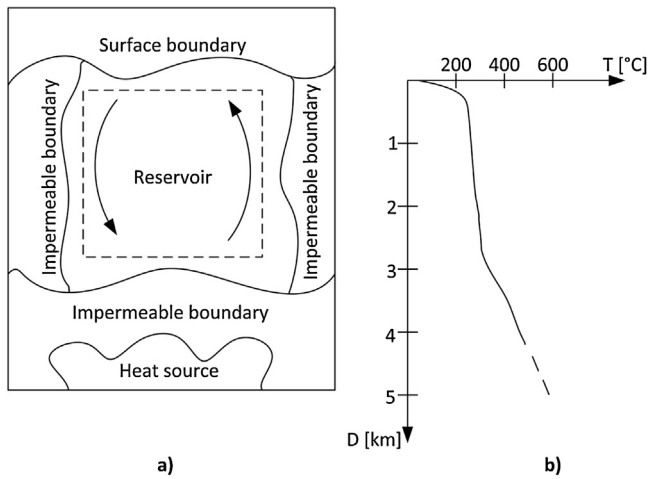*E-mail address:* msg@ru.is (M. Gudjonsdottir).

Fig. 1. (a) A conceptual representation of a two phase convective geothermal system and (b) temperature profile for the different layers of the system.
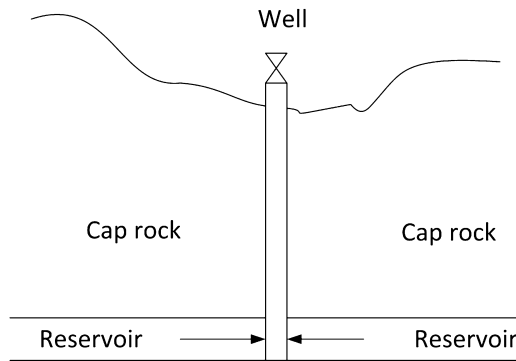

Fig. 2. A figure showing where a geothermal well is drilled into a reservoir, causing fluid to flow through the fractured reservoir into the well.

permeabilities are plotted vs. the water saturation in Figs. 3 and 4. A summary of measurements and saturation techniques can also be found in a paper by Horne et al. (2000). As seen from Figs. 3 and 4 no fundamental set of curves describing the relative permeabilities seems to exist for the case of water and steam.

According to previous research on two phase flow in fractured material, the relative permeabilities of flow in fractured material do not show a clear deviation from the relative permeabilities for flow in porous materials. There seems to be phase interference for two phase flow through fractures as well as through porous material (Chen, 2005; Diomampo, 2001). A wide range of relative permeability functions are available for simulations of two phase flow through fractured as well as porous materials (Pruess et al., 1999; Kipp et al., 2008). Porous homogeneous materials can however give

Table 1
Summary of experiments found in the literature for evaluating relative permeabilities of water and steam, d, inner diameter of flow channel; L, length of flow channel; k, intrinsic permeability.

Reference	Filling	Dimensions
Ambusso (1996), Mahiya (1999), Satik (1998), and O'Connor (2001)	Berea sandstone core $k = 0.6$ D	$d = 5.08$ cm $L = 43.2$ cm
Piquemal (1994)	Unconsolidated quartz sand $k = 3.78–3.96$ D	$d = 5$ cm $L = 25$ cm
Verma (1986)	Glass bead $k = 0.64$ D	$d = 7.62$ cm $L = 100$ cm
Sanchez et al. (1986) Sanchez and Schechter (1990)	Silica sand $k = 7.3$ D	$d = 3.18$ cm $L = 19.5$ cm

Table 2
A sample of relative permeability functions from TOUGH2 reservoir simulator (Pruess et al., 1999) as functions of the normalized water saturation S_{wn}.

Name (Reference)	k_{rw}	k_{rs}
X-curves	S_{wn}	$1 - S_{wn}$
Corey curves (Corey, 1954)	S_{wn}^4	$(1 - S_{wn})^2(1 - S_{wn}^2)$
Grants curves (Grant, 1977)	S_{wn}^4	$1 - k_{rw}$
Functions of Fatt and Klikoff (Fatt and Klikoff, 1959)	S_{wn}^3	$(1 - S_{wn})^3$
Functions of Verma (Verma, 1986)	S_{wn}^3	$1.259 - 1.7615 S_{wn} + 0.5089 S_{wn}^2$

easily characterizable measure of the relative permeabilities that can be transferred to other configurations like fractured material.

The relative permeabilities are important parameters in reservoir modeling. They are not only used to calculate the mass flux or the velocity of the phases but also for estimating thermodynamic and transport properties and can affect the parameters related to the reservoir performance significantly (Bodvarsson et al., 1980). A number of relative permeability functions used in the numerical reservoir simulator TOUGH2 (Pruess et al., 1999) are listed in Table 2 and indicate the wide range of relative permeability functions used in practice in such simulators. The relative permeability functions in Table 2 are presented as functions of the normalized water saturation, S_{wn} which defines the mobile region of the phases.

The higher degree of the polynomials in Table 2 imply that more interaction occurs between the two phases. When results of steam and water flow are compared to nitrogen–water flow or air–water flow using the same experimental setup, the relative permeabilities for the steam phase seem to be higher than for the nonwetting phase (at the same water saturation) for the air–water and nitrogen–water experiments (Chen, 2005; Chen et al., 2007). That indicates that the boiling mechanism induces the flow of the steam where in absence of boiling the two phases seem to restrain the flow of each other to a greater extent.

More information is needed regarding the two phase flow of water and steam in porous medium. The purpose of this study was to address this need by performing an experiment where two phase mixture of a geothermal fluid was injected into relatively large tube filled with porous material. The dimensions of the tube were selected to reduce the end and wall effects of the device. The conditions may therefore to some extent resemble a geothermal reservoir better than in many of the previous experiments.

2. Methods and materials

2.1. Theoretical background

Eq. (1) states Darcy's law for a steady state, incompressible single phase flow with mass flux $\bar{q}$ of a fluid with kinematic viscosity ν and density ρ flowing through a permeable matrix with intrinsic permeability k and where ∇p is the pressure gradient and g is the gravitational acceleration.

$$\bar{q} = -\frac{k}{\nu}(\nabla p - \rho \bar{g}) \tag{1}$$

This law is applicable for a laminar flow at relatively low Reynolds numbers defined in Eq. (2).

$$Re = \frac{\nu L}{\nu} \tag{2}$$

Where ν is the local velocity of the fluid and L is the characteristic flow dimension. For a flow in a porous media, the characteristic dimension used in Eq. (2) is the effective grain size d_e. Various determinations of the effective grain size are found in the literature,
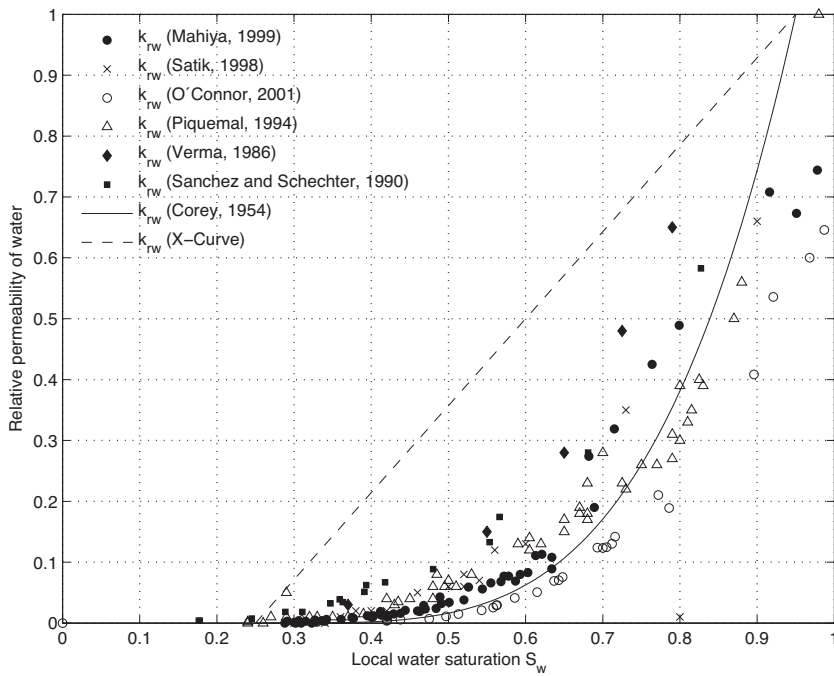
Fig. 3. Summary of experimental results of relative permeabilities for water together with the Corey (1954) and the X-curve with residual saturations $S_{wr} = 0.25$ and $S_{sr} = 0.05$.

usually they range between 10% (Todd and Mays, 2005) and 30% of the passing sieve diameter. Darcy's law is applicable for $Re < 1$ and this limit has in some cases been extended up to 10 or higher (Zeng and Grigg, 2006). Thus, the limit is not general, and for a given flow case, a linearity between the mass flux and the pressure gradient has to be assured for Eq. (1) to be valid.

Darcy's law from Eq. (1) is not sufficient for a two phase flow, and must be modified. A modified version of Darcy's law for a one dimensional two phase flow of water and steam, which is the subject of this study, is shown below in Eqs. (3) and (4). Where the

subscripts w and s denote water and steam respectively with k_{rw} and k_{rs} denoting their relative permeabilities.

$$\vec{q}_w = -\frac{kk_{rw}}{v_w}\left(\frac{dp}{dz} - \rho_w\vec{g}\right) \tag{3}$$

$$\vec{q}_s = -\frac{kk_{rs}}{v_s}\left(\frac{dp}{dz} - \rho_s\vec{g}\right) \tag{4}$$
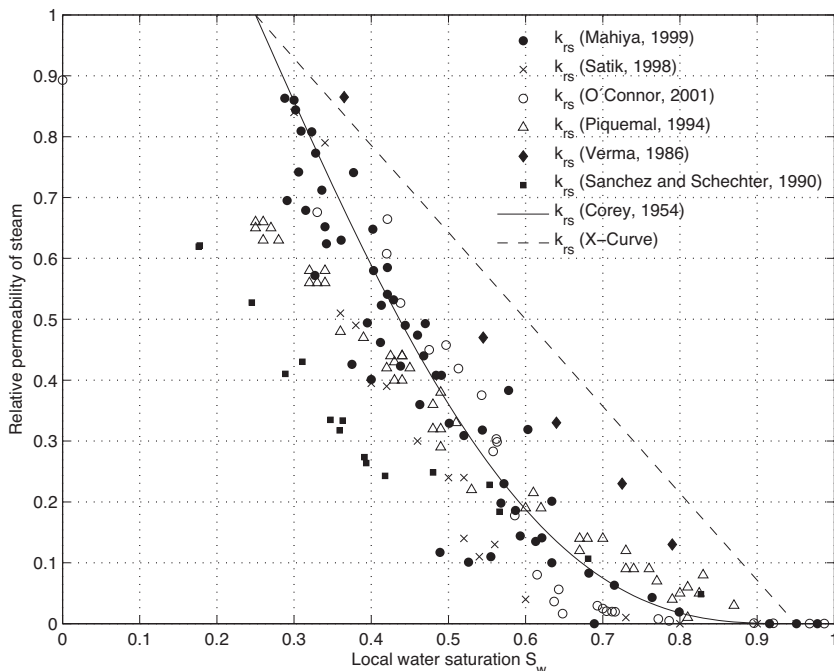

Fig. 4. Summary of experimental results of relative permeabilities for steam together with the Corey (1954) and the X-curve with residual saturations $S_{wr} = 0.25$ and $S_{sr} = 0.05$.

Table 3
Description of the components of the measurement device referring to Fig. 5.

Component	Component name	Description
A	Stop valve	$D = 1$ in.
B	Throttle valve	$D = 1$ in.
C	Pressure sensor/pressure indicator	Tecsis 4–20 mA/indicator
D	Temperature sensor	Thermocouple
E	Pipe filled with porous material	$D = 10$ in., $t = 5$ mm, $L = 4$ m
F	Back pressure valve	$D = 1$ in.
G	Condenser/cooler	Heat exchanger
H	Flow meter	Mass and time measurement

Scheidegger (1974) derived an expression for Darcy's law for the steam phase taking the compressibility effect of the gas into account, shown in Eq. (5).

$$q_s = -\frac{k k_{rs}(p_{in}^2 - p_{out}^2)}{v_s 2 p_{out} \Delta L} \tag{5}$$

Where p_{in} and p_{out} are the inlet and outlet pressures in a permeable interval of a flow channel of length ΔL.

The relative permeabilities are normally introduced as a pair of curves depending on the normalized water saturation only (Pruess et al., 1999) as shown in Table 2. The normalized water saturation defines the mobile region of the two phases as shown in Eq. (6)

$$S_{wn} = \frac{S_w - S_{wr}}{1 - S_{sr} - S_{wr}} \tag{6}$$

The residual saturations, S_{wr} and S_{sr} are the limits of the mobile region. The local water saturation, S_w is defined as shown in Eq. (7) for a control volume $V_w + V_s$.

$$S_w = \frac{V_w}{V_w + V_s} \tag{7}$$

When the local water saturation is not known and cannot be measured, like is normally the case for geothermal reservoirs, the flowing water saturation, $S_{w,f}$ which is defined in Eq. (8) can be used for comparison.

$$S_{w,f} = \frac{\dot{Q}_w}{\dot{Q}_w + \dot{Q}_s} = \frac{(1-x)v_w}{(1-x)v_w + x v_s} \tag{8}$$

Where $\dot{Q}_w$ and $\dot{Q}_s$ are the volumetric flows of water and steam respectively and v_w and v_s are the specific volumes of water and steam respectively and x is the steam fraction as defined in Eq. (9).

$$x = \frac{\dot{m}_s}{\dot{m}_s + \dot{m}_w} \tag{9}$$

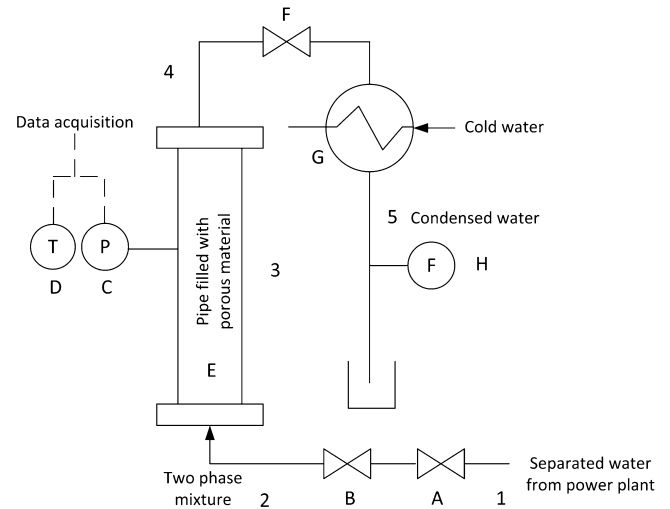Here, $\dot{m}_w$ and $\dot{m}_s$ are the mass flows of water and the steam respectively.

Reyes et al. (2004) compared local saturation to the flowing saturation, gaining the relation shown in Eq. (10) which they used to obtain the local saturation for relative permeabilities from field data.

$$S_w = 0.1152 \ln(S_{w,f}) + 0.8588 \tag{10}$$

In this work, the equations from this section were used to calculate the relative permeabilities from directly measured values. The measurements were made using the equipment described in Section 2.2.

2.2. Experimental setup and procedure

A process diagram of the measurement device is shown in Fig. 5 and the components are described in the equipment list in Table 3. The main component was an insulated steel pipe (component E in

Fig. 5. A process diagram showing the main components and fluid states in the measurement device designed and constructed for this study. The components are described in Table 3.

Table 3 and Fig. 5) filled with porous material. It had flanges on each end, enabling change of filling material. The pipe was supported on a bracket enabling rotation so the flow direction could be changed. Fig. 6 shows a photo and a 3D drawing of the experimental device.

The fluid used for the experiments was of geothermal origin flowing from separators at Reykjanes geothermal power plant (HS-Orka, 2014). The reservoir fluid at the Reykjanes geothermal field is hydrothermally altered seawater with magmatic gases and high in salinity (Arnorsson, 1978; Fridriksson et al., 2010). The seawater near the coast of Reykjanes has chloride (Cl) concentration of 19,100 mg/kg and the Reykjanes wells have Cl concentration ranging from 18,000 to 21,000 mg/kg (Fridriksson et al., 2010) or 3.2 wt% NaCl (Hardardottir et al., 2010). The average silica (SiO_2) concentration in the Reykjanes wells is 665 mg/kg (Hardardottir et al., 2010). The fluid used for the experiments flowed from the steam separator in the power plant as saturated water at 210 °C and 19 bar$_a$. The turbines in the power plant are operated at this inlet pressure which is unusually high compared to other geothermal power plants (Yamaguchi, 2010). The reason for the high separation and turbine inlet pressure is due to silica scaling prevention. For lower separation pressures it is more likely that serious silica scaling issues arise. The reservoir fluid temperature is up to 315–320 °C (Freedman et al., 2009; Hardardottir et al., 2009) which according to the amorphous silica (Fournier and Rowe, 1977) and quartz (Fournier and Potter, 1982) solubility curves will result in silica scaling to occur at separation temperatures above 200 °C. The effect of salinity however results in higher silica solubility (Von Damm et al., 1991) but same temperature limits for silica prevention are expected.

The separated fluid was used to produce a two phase mixture in a throttle valve (component B) by lowering the pressure, as shown in the p–h diagram in Fig. 7. The fluid used for the experiments flowed through an approximately 20 m long pipeline from the separator to the device. Even though the pipeline was well insulated a considerable heat loss occurred on the way. The enthalpy at the device inlet (state 2 in Fig. 5) was measured with a tracer analysis method described by Lovelock (2001) and was 855 kJ/kg. The enthalpy therefore decreased from 890 kJ/kg, which was the saturation condition in the separator, due to heat loss in the pipeline.

After a two phase mixture was formed in the throttle valve (component B) it was injected into the pipe (component E). As the two phase mixture flowed through the resistive filling its

Fig. 6. A photo showing the experimental setup and a 3D drawing showing the pipe on the steel bracket.
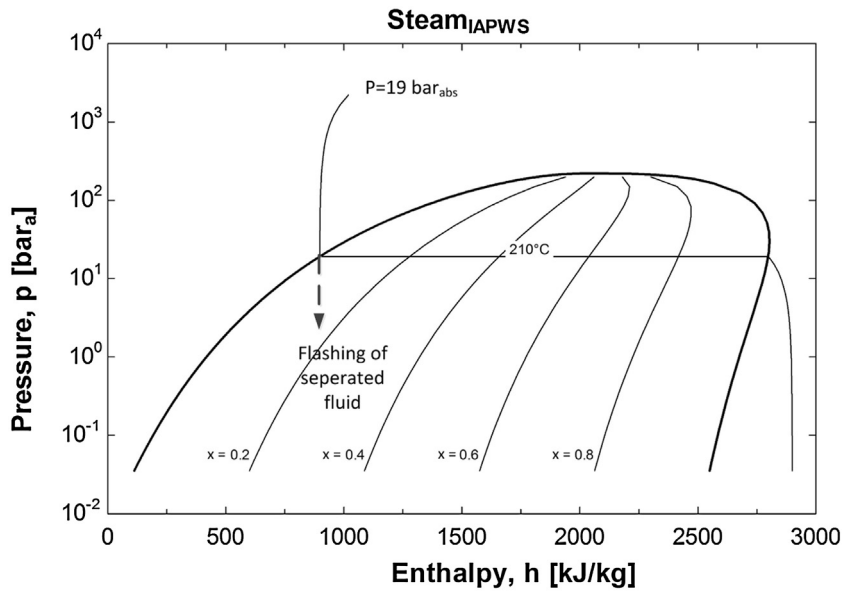

Fig. 7. Pressure–enthalpy diagram for water, using the IAPWS database (IAPWS, 2007).

pressure decreased. The fluid pressure was measured and logged at four locations on the pipe, see Fig. 8. As the pressure was logged continuously it could be observed when steady state condition of the flow was reached.
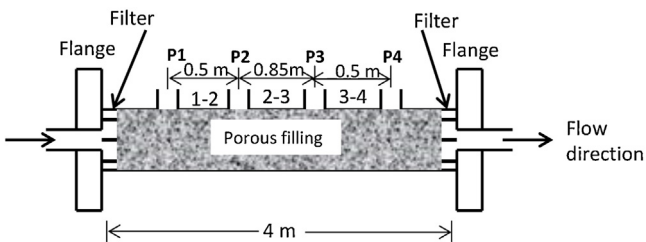

Fig. 8. Location of pressure sensors on the measurement device.

At the exit of the pipe (state 4 in Fig. 5) a valve (component F) was installed to control the back pressure. The condenser (component G) condensed the two phase mixture exiting the device and a manual flow measurement (component H) was made for the condensed water to determine the total mass flow, $\dot{m}_{tot}$ through the pipe. The condenser consisted of a pipe, which the two phase mixture was flowing through, immersed in a cold water tank. To determine the mass flow of each phase Eqs. (11) and (12) were used.

$$\dot{m}_w = (1-x)\dot{m}_{tot} \tag{11}$$

$$\dot{m}_s = x\dot{m}_{tot} \tag{12}$$

The steam fraction x was calculated using Eq. (13).

$$x = \frac{h_t - h_w}{h_s - h_w} \tag{13}$$

Table 4
List of setups for the measurements, the vertical flow was upwards against gravity.

Setup	Filling type	Direction
1. Sand	Crushed basalt 0–2 mm grain size	Vertical
2. Sand	Crushed basalt 0–2 mm grain size	Horizontal
3. Sand and gravel	Crushed basalt 0–5 mm grain size	Vertical
4. Sand and gravel	Crushed basalt 0–5 mm grain size	Horizontal

where h_w and h_s are the saturation enthalpies for water and steam respectively calculated from the measured pressure values P1–P4 in Fig. 8. h_t is the total enthalpy of the fluid according to the measured enthalpy.

The intrinsic permeability, k, of the porous filling inside the pipe had to be determined for the relative permeability calculations according to Eqs. (3) and (4). It was measured using single phase water from the condenser outlet in the power plant. The available condensed water was at 40 °C and 19 bar$_a$. By using Eq. (1) the intrinsic permeability could finally be determined.

With the collected data, that is the pressure at locations P1–P4 in Fig. 8, the total mass flow measurement, the measured intrinsic permeability and phase mass flow determinations from Eqs. (11) and (12), the relative permeabilities could be calculated using Eqs. (3) and (4) as shown in Eqs. (14) and (15) where the body forces $\rho_w g$ and $\rho_s g$ applied only to the vertical flow cases.

$$k_{rw} = -\frac{(\dot{m}_w/A)v_w}{k((\Delta p/\Delta L) + \rho_w g)} \qquad (14)$$

$$k_{rs} = -\frac{(\dot{m}_s/A)v_s}{k((\Delta p/\Delta L) + \rho_s g)} \qquad (15)$$

where $(\Delta p/\Delta L)$ is the measured pressure gradient of the two phase flow and A is the area of the flow channel. Here, the capillary pressures are considered to be negligible and the same pressure applies for both phases at each location P1–P4.

After the measurement device was initially run with cold water to determine the intrinsic permeability, it was run with a two phase mixture using four different setups, listed in Table 4. Measurements for each setup were conducted multiple times with different inlet pressure and mass flow. The intrinsic permeability was measured between the runs to see if it had changed during the two phase runs. This was then repeated for all the setups listed in Table 4.

3. Results

3.1. Intrinsic permeability measurements

Before being able to calculate the relative permeabilities, the intrinsic permeability was calculated from the measured values of water phase only. The results are shown in Figs. 9 and 10. The intervals defined in Figs. 9 and 10 are related to pressure ports P1–P2 (Int 1–2), P2–P3 (Int 2–3) and P3–P4 (Int 3–4) seen in Fig. 8 with the results separated based on the four experiments setups listed in Table 4. The plots show the mean value of the intrinsic permeabilities and the error bars are two standard deviations in total.

3.2. Relative permeability measurements

The intrinsic permeabilities were then used to calculate the relative permeabilities, taking into account the variance in the intrinsic permeability. The relative permeabilities for the two phase flow were calculated according to the methods described in Section 2.2 by using the measured values and Eqs. (14) and (15). The results obtained by using Eq. (5) were also considered but did not lead to considerable differences. Note that the water saturation could not be measured directly in this experiment. Plots of the relative permeabilities similar to Figs. 3 and 4 could therefore not be made. For

comparison purposes the two relative permeabilities were plotted in Fig. 11 for the setups listed in Table 4 together with the X curve, the Corey curve (Corey, 1954) and the Functions of Verma (Verma, 1986).

Although the local water saturation was not known, the flowing saturation defined in Eq. (8) could be determined. The relative permeabilities were plotted as functions of the flowing saturations as shown in Fig. 12 for the setups listed in Table 4.

By using the relation shown in Eq. (10) connecting the flowing saturation S_{wf} and the local water saturation S_w, the local water saturation could be estimated and the relative permeabilities compared to relative permeability curves as seen in Fig. 13. Fig. 14 shows the cases where the pipe was filled with sand only.
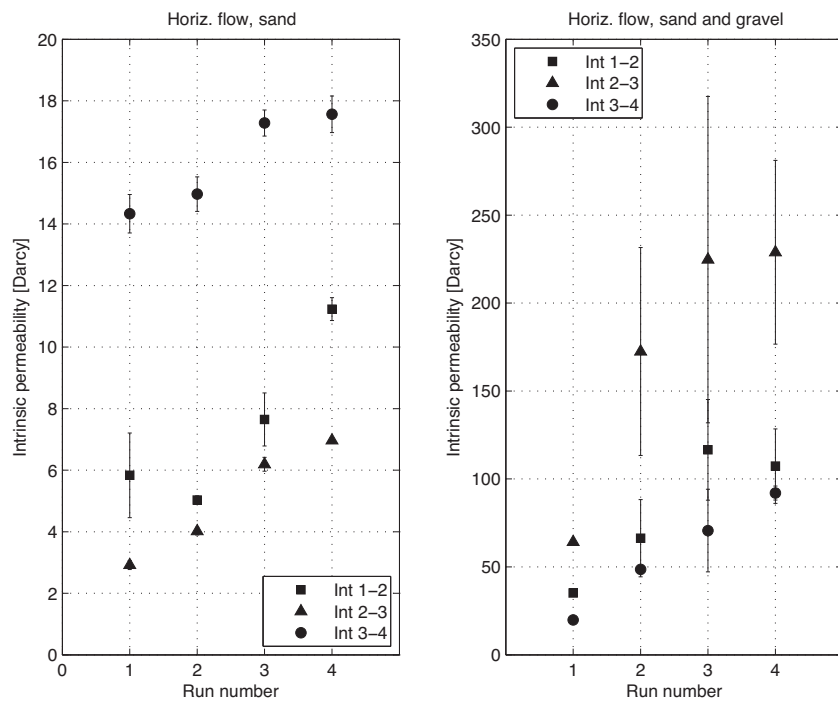
4. Discussion

In this paper, the methods and results of measurements and calculations of relative permeabilities for a two phase mixture of water and steam are described. The measurements were performed in a large scale laboratory device using fluid of a geothermal origin, therefore resembling real geothermal situations better at laboratory conditions than previous measurements have.

The results in Fig. 11 show that the relative permeabilities deviate from the X curves, therefore supporting the idea that they are not linearly dependant on water saturation. The results also show, that for most of the values, the calculated relative permeabilities are located between the Corey curves and the Functions of Verma. That indicates that the phase interaction is smaller than proposed by the Corey curves but higher than proposed by the Functions of Verma.

The results do not indicate a uniform function as a correlation between the relative permeabilities. The relative permeabilities form a scattered cloud instead of a clear line such as a relative permeability curve. One of the main factors contributing to the errors in the experimental procedure is the determination of the intrinsic permeabilities as seen in Figs. 9 and 10 which show a large variance in the intrinsic permeabilities.
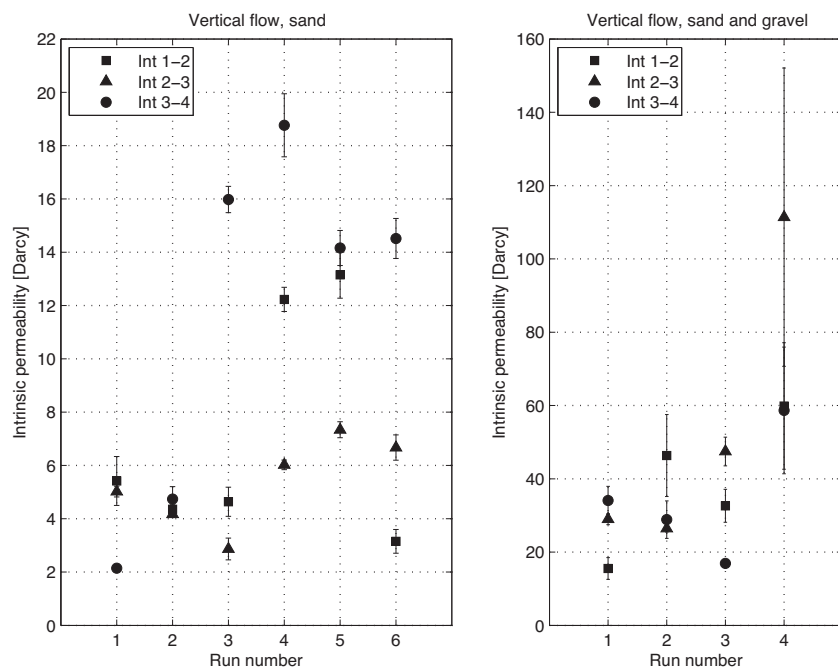
Although the intrinsic permeabilities were calculated between the two phase runs, and a new value gained for each run, there still was a variance in the intrinsic permeability. As shown in Fig. 9 for the horizontal setup, the intrinsic permeability increased with each run, however as shown in the left part of Fig. 10 for the vertical flow the intrinsic permeability increased after the first runs and then decreased. That might result from the different packing distribution or scaling occurring mainly at specific locations in the pipe. The variance in the intrinsic permeabilities may also be due to the fact that some of the smaller particles in the filling were washed out through the filter holding the porous material in place, thereby increasing the intrinsic permeability between runs. When the brine was flashed through the pipe its pressure and correspondingly the temperature decreased to values below the temperature limit for silica scaling to occur. When the pipe was emptied silica scaling could be observed within the porous material that the pipe was filled with. This nature of silica precipitation in porous material is known in geothermal applications. Silica precipitation rate in porous materials has been reported in order to predict the effect of it for reinjection sites. In a study by Mroczek et al. (2000) the silica deposition rates were measured experimentally and the results used for predicting the effect of injecting brine into the reservoir at Wairakei. The results predicted a permeability reduction in the vicinity of the well. This behavior was detected for vertical flow through the smaller grain size. For other flow cases other factors changing the intrinsic permeability, like the packing distribution, seem to have had a larger effect.

Fig. 9. Result of measurements of the intrinsic permeabilities for sand (left) and sand–gravel (right) filled column, for horizontal flow direction. Number of runs correlated with increasing time.

The data points for setups 3 and 4 (see Table 4) where filling material with larger grain size was used, shows high variance in the relative permeabilities. The stability of the intrinsic permeability was also low for that filling type as seen in Figs. 9 and 10 which results in higher error factors in the calculation of relative permeabilities. Fig. 14 can therefore be compared to Fig. 13 showing less variance of the relative permeabilities when only results using sand are shown.

Although these error factors may result in less detailed results, the measurements show a resemblance to a real geothermal reservoir since the geothermal fluid normally does not flow at controlled conditions in the reservoir. Factors like precipitation of minerals and varying intrinsic permeability are likely to be observed in real cases. In Fig. 12 the relative permeabilities follow a pattern where water relative permeabilities increase with the flowing saturation $S_{w,f}$ and the relative permeabilities of steam decreases with

Fig. 10. Result of measurements of the intrinsic permeabilities for sand (left) and sand–gravel (right) filled column, for vertical flow direction. Number of runs correlated with increasing time.
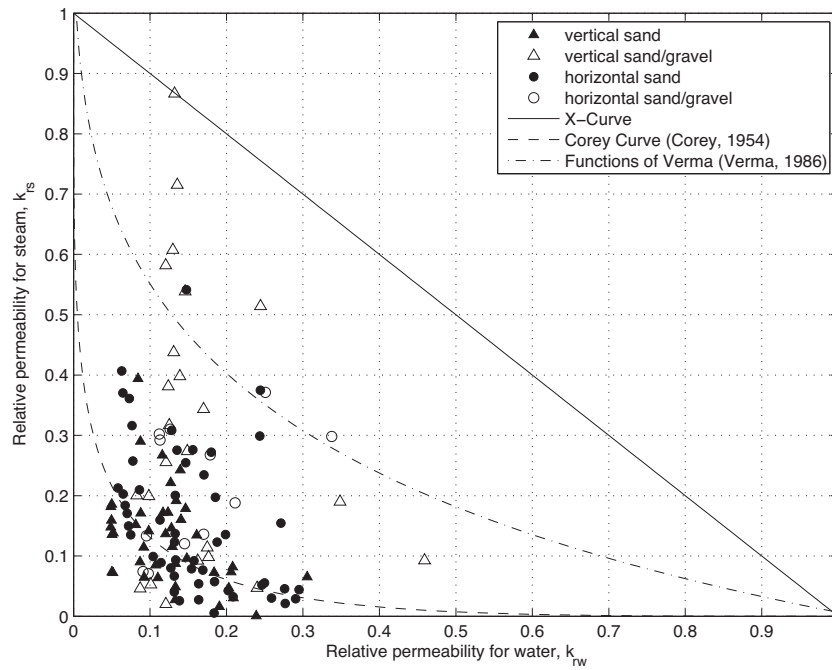
Fig. 11. Calculated relative permeabilities from the experimental measurements, compared with results from literature.

increasing $S_{w,f}$. When the local water saturation was determined using Eq. (10) the relative permeabilities shown in Fig. 13 shift in the saturation range from Fig. 12 indicating that the flowing saturation is underestimated. That was also the result in a previous research (Reyes et al., 2004).

As seen in Fig. 11 no clear difference is seen between the relative permeabilities if the flow direction is horizontal or vertical. That does not necessarily mean that the flow direction is not affecting them. In this setup the pressure gradient was an order of magnitude higher than the body force due to gravity, leading to only small

effects of the gravity on the overall measurements according to Eqs. (3) and (4).

In Fig. 11 it can be observed, that the relative permeabilities of water appear to be almost constant for higher values of the steam fraction x. The reason can be that with increasing steam content, the velocity increases due to lower density of the mixture. The fluid might push the grains of which the filling consists to the side, leading to higher intrinsic permeabilities which is then not accounted for when calculating the relative permeabilities. Using higher values of the intrinsic permeabilities for these points (where
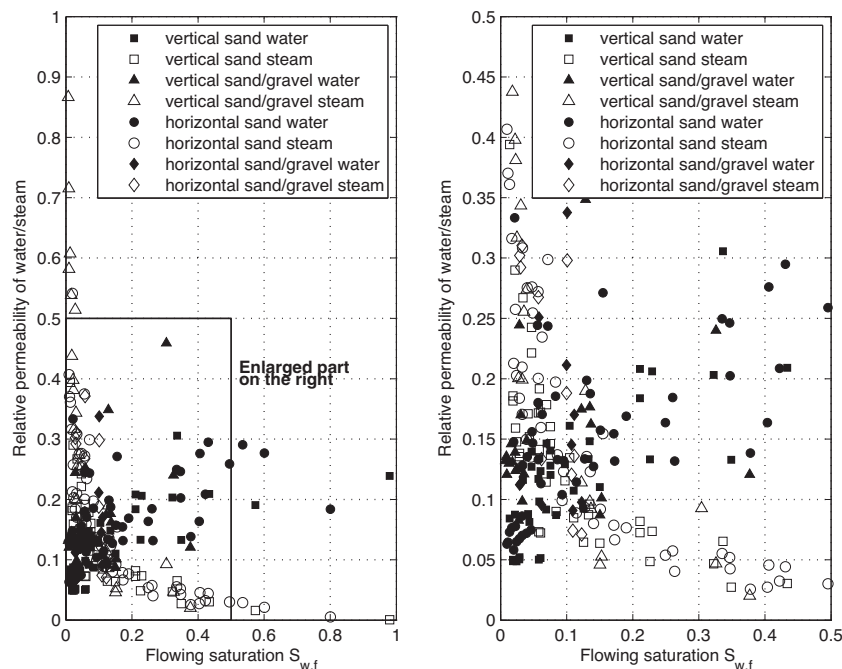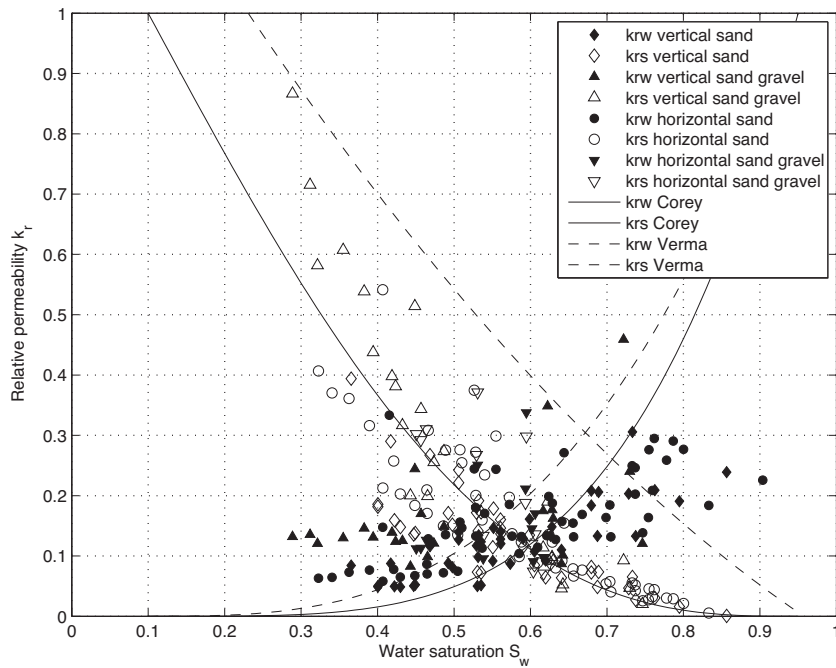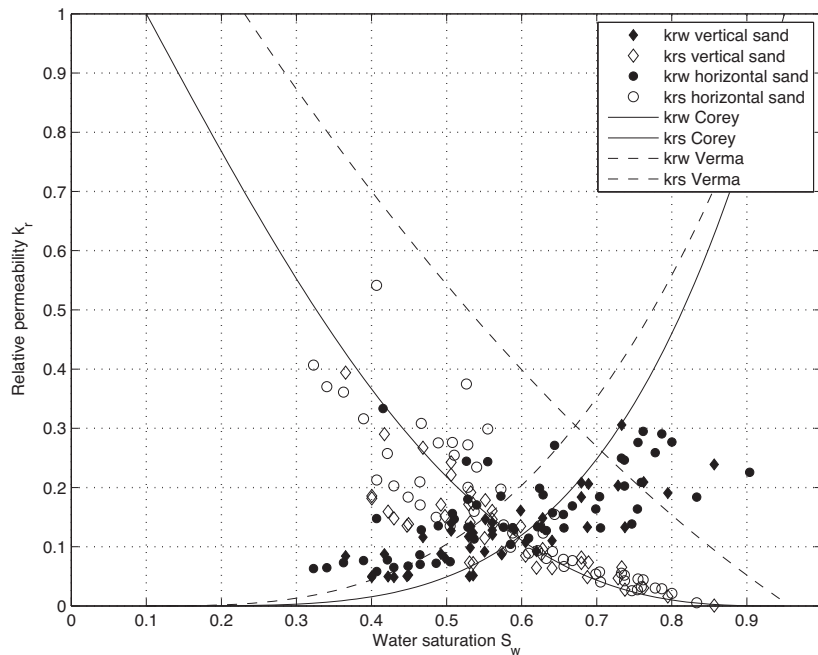

Fig. 12. The relative permeabilities from Fig. 11 as functions of the flowing saturations, the graph on the right side is an enlarged part of the graph on the left side.

Fig. 13. The calculated relative permeabilities as functions of the local saturation, gained from Eq. (10) for all four flow cases listed in Table 4. For the Corey and the Verma curves $S_{wr} = 0.1$ and $S_{sr} = 0.05$.

Fig. 14. The calculated relative permeabilities as functions of the local saturation for the cases shown in Fig. 13 where the device was filled with sand.

the water saturation is low) would result in lower relative permeabilities.

In Fig. 13 the steam relative permeabilities follow the Corey curve quite well, but the water relative permeabilities do not. For lower water saturations the error in intrinsic permeabilities measurements might have resulted in larger relative permeabilities of water due to the reasons as already stated. For larger water saturations the relative permeabilities of water are however lower than the Corey curves. This indicates that there is more interaction among these values than predicted by the Corey curves.

5. Conclusions

The main conclusions of the paper can be summarized as follows:

- The conditions in this experiment are likely to resemble the flashing of geothermal fluid from water phase to steam phase as occurs in liquid dominated systems.
- The relative permeabilities calculated from measured values show deviation from the linear curves, therefore they indicate an interaction between the two phases.

- Most of the resulting relative permeabilities are located between the Corey curves and the Functions of Verma, therefore indicating less interaction between the phases than predicted by the Corey curves and more interaction than the Functions of Verma indicate.
- Variability of intrinsic permeabilities are considered to be the main error source in the calculations since the effect of silica scaling and nonuniform packing along the test column was detected.
- In real geothermal reservoirs, the intrinsic permeabilities can hardly be considered constant, therefore reservoir behavior resembling the results shown here might be expected for real geothermal cases.
- Since the pressure gradient was an order of magnitude higher than the body force due to gravity, there was not a detectable difference between the relative permeabilities if the flow direction was parallel or perpendicular to the gravity field.
- When the results are presented using the local water saturation, as calculated from the flowing saturation, the relative permeabilities show behavior similar to known functions. This applies however only to the steam phase.

Acknowledgements

References

Ambusso, W., 1996. Experimental determination of steam water relative permeability relations. M.Sc. thesis, Stanford University, California.

Arnorsson, S., 1978. Major element chemistry of the geothermal sea-water at Reykjanes and Svartsengi, Iceland. Mineral. Mag. 42, 209–220, http://dx.doi.org/10.1180/minmag.1978.042.322.07.

Arnorsson, S., Stefansson, A., Bjarnason, J., 2007. Fluid–fluid interactions in geothermal systems. Rev. Mineral. Geochem. 65, 259–312, http://dx.doi.org/10.2138/rmg.2007.65.9.

Axelsson, G., 2008. Production capacity of geothermal systems. In: Workshop for Decision Makers on Direct Heating Use of Geothermal Resources in Asia, organized by UNU-GTP, TBLRREM and TBGMED, Tianjin, China 11–18 May.

Bodvarsson, G., O'Sullivan, M., Tsang, C., 1980. The sensitivity of geothermal reservoir behavior to relative permeability parameters. In: Proc. 6th Workshop on Geothermal Reservoir Engineering, Stanford University, Stanford, California, pp. 224–237.

Chen, C.Y., 2005. Liquid–gas relative permeabilities in fractures: effects of flow structures, phase transformation and surface roughness. Stanford University, Stanford, California.

Chen, C.Y., Horne, R., 2006. Two-phase flow in rough-walled fractures: experiments and a flow structure model. Water Resour. Res. 42, W03430, http://dx.doi.org/10.1029/2004WR003837.

Chen, C.Y., Horne, R., Fourar, M., 2004. Experimental study of liquid–gas flow structure effects on relative permeabilities in a fracture. Water Resour. Res. 40, W08301, http://dx.doi.org/10.1029/2004WR003026.

Chen, C.Y., Li, K., Horne, R., 2007, October. Experimental study of phase-transformation effects on relative permeabilities in fractures. SPE Reserv. Eval. Eng., 514–526.

Corey, A., 1954. The interrelation between gas and oil relative permeabilities. Producers Monthly 19, 38–41.

Diomampo, G., 2001. Relative permeability through fractures. M.Sc. thesis, Stanford University, Stanford, California.

DiPippo, R., 2008. Geothermal Power Plants. Elsevier Ltd.

Fatt, I., Klikoff, W., 1959. Effect of fractional wettability on multiphase flow through porous media. AIME Trans., 216–246.

Fournier, R., Potter, R., 1982. A revised and expanded silica (quartz) geothermometer. Geotherm. Resour. Counc. Bull. 11, 3–12.

Fournier, R., Rowe, J., 1977. The solubility of amorphous silica in water at high temperatures and pressures. Am. Mineral. 62, 1052–1056.

Freedman, J., Bird, D., Arnorsson, S., Fridriksson, T., Elders, W., Fridleifsson, G., 2009. Hydrothermal minerals record CO_2 partial pressure in the Reykjanes geothermal system, Iceland. Am. J. Sci. 309, 788–833, http://dx.doi.org/10.2475/09.2009.02.

Fridriksson, T., Oladottir, A., Jonsson, P., Eyjolfsdottir, E., 2010. The response of the Reykjanes geothermal system to 100 MWe power production: fluid chemistry and surface activity. In: Proceedings World Geothermal Congress 2010, Bali, Indonesia, 25–29 April.

Grant, M., 1977. Permeability reduction factors at Wairakei. In: Paper 77-HT-52, presented at AICHE-ASME, Heat Transfer Conference, Salt Lake City, Utah, August 1977.

Grant, M., Bixley, P., 2011. Geothermal Reservoir Engineering, second ed. Academic Press.

Hardardottir, V., Brown, K., Fridriksson, T., Hedenquist, J., Hannington, M., Thorhallsson, S., 2009. Metals in deep liquid of the Reykjanes geothermal system, southwest Iceland: implications for the composition of seafloor black smoker fluids. Geology 37, 1103–1106, http://dx.doi.org/10.1130/G30229A.1.

Hardardottir, V., Hedenquist, J., Hannington, M., Brown, K., Fridriksson, T., Thorhallsson, S., 2010. Composition of reservoir liquid and metals in pipeline scale, Reykjanes geothermal system, SW Iceland. In: Proceedings World Geothermal Congress 2010, Bali, Indonesia, 25–29 April.

Horne, R., Satik, C., Mahiya, G., Li, K., Ambusso, W., Tovar, R., Wang, C., Nassori, H., 2000. Steam–water relative permeability. In: Proc. World Geothermal Congress 2000, Kyushu–Tohoku, Japan, May 28–June 10.

HS-Orka, 2014. Website http://www.hsorka.is/english/hsproduction/hsproductionreykjanesvirkjun.aspx (accessed 16.03.14).

The international association for the properties of water and steam (IAPWS), 2007. Revised Release on the IAPWS Industrial Formulation 1997 for the Thermodynamic Properties of Water and Steam. Technical Report August 2007, Lucerne, Switzerland.

Kipp, K., Hsieh, P., Charlton, S., 2008. Guide to the revised ground-water flow and heat transport simulator: HYDROTHERM version 3. U.S. Geological Survey, Reston, Virginia.

Lovelock, B., 2001. Steam flow measurement using alcohol tracers. Geothermics 30, 641–654, http://dx.doi.org/10.1016/S0375-6505(01)00020-7.

Mahiya, G., 1999. Experimental measurement of steam–water relative permeability. M.Sc. thesis, Stanford University, Stanford, California.

Mroczek, E., White, S., Graham, D., 2000. Deposition of amorphous silica in porous packed beds predicting the lifetime of reinjection aquifers. Geothermics 29, 737–757, http://dx.doi.org/10.1016/S0375-6505(00)00027-4.

O'Connor, P., 2001. Constant-pressure measurement of steam–water relative permeability. M.Sc. thesis, Stanford University, Stanford, California.

O'Sullivan, M., Pruess, K., Lippmann, M., 2001. State of the art of geothermal reservoir simulation. Geothermics 30, 395–429, http://dx.doi.org/10.1016/S0375-6505(01)00005-0.

Piquemal, J., 1994. Saturated steam relative permeabilities of unconsolidated porous media. Transport Porous Med. 17, 105–120, http://dx.doi.org/10.1007/BF00624727.

Pruess, K., Oldenburg, C., Moridis, G., 1999. TOUGH2 User's Guide, Version 2.0. Earth Sciences Division, Lawrence Berkeley National Laboratory, University of California, Berkeley, California.

Reyes, J., Chen, C.Y., Li, K., Horne, R., 2004. Calculation of steam and water relative permeabilities using field production data, with laboratory verification. GRC Trans. 28, 609–615.

Sanchez, J., Schechter, R., 1990. Steady adiabatic, two-phase flow of steam and water through porous media. SPE Reserv. Eng., 293–300, August 1990.

Sanchez, J., Schechter, R., Monsalve, A., 1986. The effect of trace quantities of surfactant on nitrogen/water relative permeabilities. In: Paper SPE 15446 presented at the 1986 SPE Annual Technical Conference and Exhibition, New Orleans, October 5–8.

Satik, C., 1998. A measurement of steam–water relative permeability. In: Proc. 23rd Workshop on Geothermal Reservoir Engineering, Stanford University, Stanford, California, pp. 120–126.

Scheidegger, A., 1974. The Physics of Flow through Porous Media, third ed. University of Toronto, Toronto, Canada.

Todd, D., Mays, L., 2005. Groundwater Hydrology, third ed. John Wiley and Sons, Inc.

Verma, A., 1986. Effects of Phase Transformation of Steam–Water Relative Permeabilities. Ph.D. thesis, University of California, Berkeley.

Von Damm, K., Bischoff, J., Rosenbauer, R., 1991. Quartz solubility in hydrothermal seawater: an experimental study and equation describing quartz solubility for up to 0.5 M NaCl solutions. Am. J. Sci. 291, 977–1007, http://dx.doi.org/10.2475/ajs.291.10.977.

White, D., 1967. Some principles of geyser activity, mainly from steamboat springs, Nevada. Am. J. Sci. 265, 641–684, http://dx.doi.org/10.2475/ajs.265.8.641.

Yamaguchi, N., 2010. Variety of steam turbines in Svartsengi and Reykjanes geothermal power plants. In: Proceedings World Geothermal Congress 2010, Bali, Indonesia, 25–29 April.

Zeng, Z., Grigg, R., 2006. A criterion for non-Darcy flow in porous media. Transport Porous Med. 63, 57–69, http://dx.doi.org/10.1007/s11242-005-2720-3.